Research Article
Photoactivity of Titanium Dioxide Foams

Maryam Jami [iD],[1] **Ralf Dillert,**[1] **Yanpeng Suo** [iD],[1] **Detlef W. Bahnemann,**[1,2] **and Michael Wark**[3]

[1]*Institut für Technische Chemie, Leibniz Universität Hannover, Callinstraße 3, 30167 Hannover, Germany*
[2]*Laboratory "Photoactive Nanocomposite Materials", Saint Petersburg State University, Ulyanovskaya Str. 1, Peterhof, Saint Petersburg 198504, Russia*
[3]*Technische Chemie, Universität Oldenburg, Carl-von-Ossietzky Str. 9-11, 26111 Oldenburg, Germany*

Correspondence should be addressed to Maryam Jami; jamimaryam@ymail.com

TiO_2 foams have been prepared by a simple mechanical stirring method. Short-chain amphiphilic molecules have been used to stabilize colloidal suspensions of TiO_2 nanoparticles. TiO_2 foams were characterized by X-ray diffraction (XRD), X-ray photoelectron spectroscopy (XPS), UV-vis absorption spectroscopy, and scanning electron microscopy (SEM). The photoassisted oxidation of NO in the gas phase according to ISO 22197-1 has been used to compare the photoactivity of the newly prepared TiO_2 foams to that of the original powders. The results showed that the photoactivity is increased up to about 135%. Foam structures seem to be a good means of improving the photoactivity of semiconductor materials and can readily be used for applications such as air purification devices.

1. Introduction

Heterogeneous photocatalysis has been used as an effective technique for the remediation of chemical wastes. Titanium dioxide (TiO_2) is one of the most frequently investigated heterogeneous semiconductor photocatalysts and has been shown to be a relatively cheap and effective material to decompose various kinds of organic and inorganic wastes in both, the liquid and the gas phase [1–4]. As one of the most promising applications, the decomposition of nitrogen oxides (NO_x) in ambient air has been studied intensively. Nitrogen oxides (mainly NO and NO_2), which are emitted from sources such as automobiles and boilers, have become a serious environmental problem in urban areas and can also cause ozone depletion, photochemical smog, and acid deposition. Substantial efforts have been undertaken to develop methods to reduce the concentration of NO and of NO_2. In particular, the photoassisted oxidation of NO_x to nitric acid (HNO_3) using TiO_2 seems to be an effective, economical, and energy saving process for the treatment of diluted NO_x [5–10].

The photocatalytic properties of TiO_2 materials do not just depend on the chemical composition but also on the geometrical microstructure [11, 12]. During the last few decades, there have been numerous reports focusing on methods to enhance the photoactivity of TiO_2 materials [13, 14]. Several research groups have been working on the doping of TiO_2 with noble metals (Au, Pd, Ag, and Pt) or nonmetal atoms (N, F, S, C). All these investigations have developed our knowledge concerning TiO_2-based photocatalysts and have generated very interesting and important results in this research area. However, in general, the TiO_2-based photocatalysts suffer from rather low quantum efficiencies because of poor photoabsorption efficiencies and weak molecular transport capabilities [5, 15–22].

Another strategy to enhance the photoactivity of TiO_2 materials is the creation of new geometrical microstructures. It has, for example, been reported that the photoactivity of TiO_2 with structural, that is, ordered porosity is higher than that of nanoparticular TiO_2 with only interparticular nanovoids. Materials with structural porosity have high surface areas, and all pores are well interconnected. The macro-
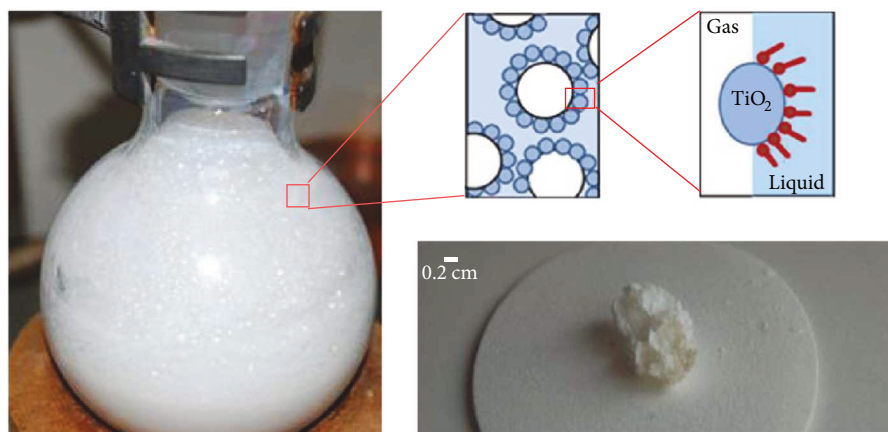
FIGURE 1: Photographs of wet particle-stabilized foams and a schematic illustration of the stabilization of gas bubbles with partially hydrophobized colloidal particles to finally obtain the TiO_2 foam.

and mesoporosity improves the adsorption and diffusion of reactants and products. The existence of cavities furthermore increases the light-capturing efficiency because of their strong light-scattering properties [21, 23–27].

Titanium dioxide foams have shown to have a higher photoactivity as the powder one by Zhao et al. [24]. However, it is not clear how the foam structure affected the photoactivity. One reason could be changes in the surface properties of TiO_2. Further investigation is necessary to confirm this theory. Photocatalytic deposition velocity is known to be an input value that predicts the possible effect of photocatalytically active surfaces on air pollution in urban areas.

In this article, it is reported that TiO_2 foams have been prepared by a simple mechanical stirring method employing short-chain amphiphilic molecules to surface-lyphobize commercially available TiO_2 nanoparticles. The aims of this work were to study the photoactivity and the changes in the surface properties of TiO_2 foams prepared in this way and compare it to that of the starting TiO_2 powder. In 2007, ISO published a standard test to evaluate the photoassisted oxidation efficiency of the air-cleaning products. The photoassisted degradation of NO in the gas phase according to ISO 22197-1 was used as the test reaction to compare the photoactivity of the TiO_2 foams to that of the original powders. Photocatalytic deposition velocities were determined to describe the changes in the surface properties. The morphology and the structural properties of TiO_2 foams have also been studied.

2. Experimental

2.1. Materials. Commercial titanium dioxide Evonik AERO-XIDE® P25 (30% rutile, 70% anatase, 20–30 nm) has been used as received. Hexylic acid (hexanoic acid) and hexylamine from Sigma-Aldrich have been used as short-chain amphiphilic molecules. Other chemicals used in the experiments were deionized water and sodium hydroxide (Sigma-Aldrich).

2.2. Foam Preparation. Titanium dioxide foams were prepared according to the method described by Zhao et al.

[24]. In short, 2 g of P25 was added stepwise to water under vigorous stirring for 20 minutes. The pH value of the suspension was around 3.6. The suspension was homogenized for about 30 min using an Ultrasonic Vibra-Cell. Meanwhile, a solution containing short-chain amphiphilic molecules (0.3 g hexylic acid in water, the ratio of TiO_2 to amphiphilic molecules was adapted from [24]), was prepared. This solution was then added dropwise to the TiO_2 suspension under vigorous stirring for 30 min.

The pH was adjusted to pH 3.5 with 0.1 M NaOH if necessary (in case of using hexylic acid as amphiphilic agent). Finally, the wet TiO_2 foam was produced and this wet foam was air dried for one day at room temperature. Figure 1 shows photographs of freshly prepared wet TiO_2 foam and of a dry one.

2.3. Characterization. The crystal structures of the samples were determined by X-ray powder diffraction at room temperature using Cu Kα radiation on a Bruker D8 Advance diffractometer in the 2θ range of 10–80°. The particle size distributions were calculated from the peak broadening of the XRD patterns using the Scherrer equation [28]. X-ray photoelectron spectroscopy (XPS) measurements were carried out using a Thermo Fisher ESCALAB 250Xi equipped with monochromatic Al-Kα X-ray source (1486.6 eV). The binding energies (BE) were referenced to the adventitious carbon contamination C 1s peak (284.8 eV). High-resolution XPS spectra of Ti 2p, O 1s, and C 1s were recorded with 10 eV pass energy, and 0.02 eV step size with 5 spectra was averaged.

A scanning electron microscope (SEM) (JEOL JSM-6700F field-emission) was used to characterize the morphology of the TiO_2 foams, and the Varian Cary 4000 UV-vis spectrophotometer was used to measure the diffuse reflectance spectra of the samples. Band gap energies were calculated by using Tauc plots resulting from the Kubelka-Munk transformation of the respective diffuse reflectance spectra. The nitrogen sorption isotherms were measured at 77 K using a Quantachrome Autosorb 3. The foam samples were outgassed in vacuum at 25°C and P25-TiO_2 at 100°C for 24 hours prior the sorption measurement. The sorption data were analyzed with the quantachrome software ASiQwin 2.0.
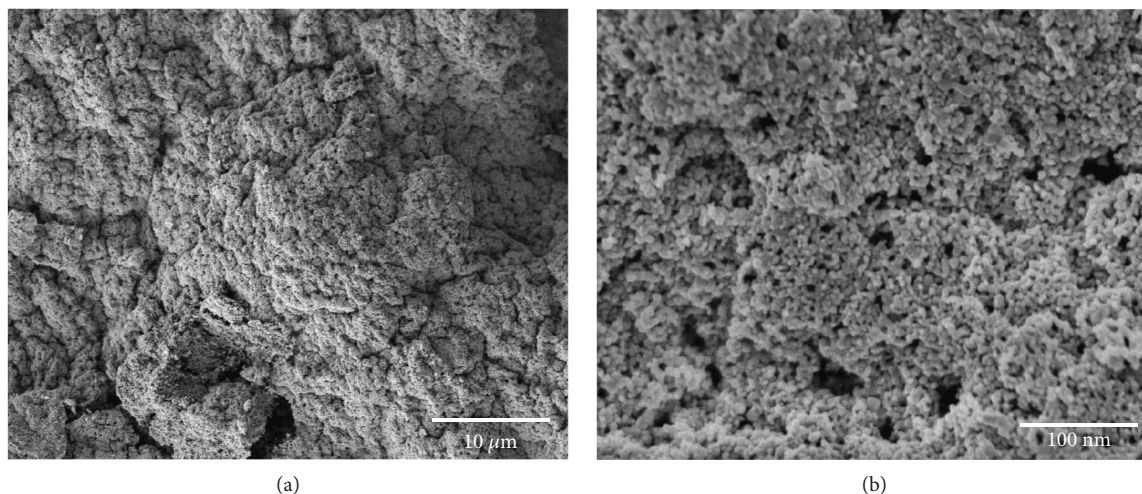
(a)

(b)

FIGURE 2: SEM pictures of the prepared TiO_2 foam with P25 as TiO_2 nanoparticle. The bar is 10 μm for the low-magnification image (a) and 100 nm for the high-magnification image (b).

2.4. Photoassisted Oxidation of NO. The photoassisted oxidation of NO was measured according to ISO 22197-1 [29]. The experimental details were described previously [9, 10, 30]. Briefly, the test equipment included the test gas supply, a humidifier, three mass flow controllers (Brooks Instrument), a photoreactor, a light source (Philips, Cleo Compact, l_{max} = 355 nm, 15 W), and a chemiluminescent $NO–NO_x$ analyzer (Horiba APNA 360). The concentration of the probe gas was followed by a NO/NO_2 analyzer in the dark until equilibrium was reached. The probe gas mixture had a concentration of 1 ppm$_v$ NO (Linde, 50 ppm$_v$ NO in N_2), a relative humidity of 50%, and a laminar volume flow $\dot{V}$ of 5×10^{-5} m^3/s. For a single degradation test, TiO_2 foam or the P25 sample was placed into the photoreactor with a geometric surface area of 18.49 cm^2 and covered with a UV(A) transparent borosilicate glass. The NO concentration was adjusted in the dark via a bypass mode followed by a dark adsorption of the pollutant on the sample surface by switching from bypass to reaction mode. After equilibration, the degradation of NO was followed under irradiation (light intensity 10 W/m^2) for 2 h until a steady state was reached. Subsequently, the system was kept in the dark until the initial concentration of NO was achieved again. For the determination of the photocatalytic deposition velocity use, a photoreactor with a geometric surface area of 39.6 cm^2 and the amount of the probe gas (NO) have been changed during the photoassisted oxidation. The NO concentration varied between 0.1 ppm$_v$ and 1.0 ppm$_v$. The flow rate of the probe gas (5×10^{-5} m^3/s), the temperature (25°C), and the relative humidity (50%) inside the photoreactor were kept constant.

3. Results and Discussions

3.1. TiO_2 Foam Characterization. The scanning electron microscopy (SEM) images of the TiO_2 foam show a porous, spongy, and rough morphology. The photograph and the low magnification image of the foam reveal macroporosity (Figure 2). The pore size distribution of the foams depends on the type of amphiphilic agent that has been used. For

example, TiO_2-foam-1 (with hexylic acid) has an average pore size of approx. 0.24 ± 0.09 cm and TiO_2-foam-2 (with hexylamine) has an average pore size of approx. 0.11 ± 0.04 cm. These large pores with extended networks provide many canals for diffusion of reactants. With increasing SEM magnification, the primary TiO_2 nanoparticles can be imaged (particle size distribution: 20–30 nm). Supplementary 1 presents the SEM photographs of TiO_2-P25, TiO_2-foam-1, and TiO_2-foam-2.

The UV-vis diffuse reflectance spectra (Supplementary Material, Fig. S2) from P25 and from the TiO_2-foam-1 have been measured, and the energy band gaps of the materials were obtained using the Kubelka-Munk function. The band gap energy of the materials was not changed ($E_g \sim 3.2$ eV) indicating that the semiconductor properties of the TiO_2 foam are same as those of the TiO_2 powder.

BET surface areas have been determined from the N_2 adsorption/desorption measurements (see Supplementary Material, Fig. S3). There is no big difference between BET surface areas of the P25 and to those of TiO_2-foam-2 (with hexylamine). P25 shows a surface area of 58.9 ± 1.8 $m^2 \cdot g^{-1}$ whereas TiO_2-foam-1 (with hexylic acid) has a surface area of 51.7 ± 1.6 $m^2 \cdot g^{-1}$ and TiO_2-foam-2 (with hexylamine) has a surface area of 58.1 ± 2.5 $m^2 \cdot g^{-1}$. Based on the experimental data, we recognize that the nitrogen sorption is not a suitable method to determine the pore size distribution of our foams. It is obvious that the TiO_2 foams have large pore size which this method could not determine.

Figure 3 shows the XRD pattern of the TiO_2 foam. This XRD pattern is, as expected, consistent with the anatase and rutile crystal phases of TiO_2 (JCPDS file number anatase: 00-0210-1272; rutile: 01-070-7347). The three characteristic sharp peaks at 2θ = 25.2°, 37.7°, and 48.0° correspond to the (101), (044), and (200) planes of the anatase phase, respectively, and the peaks at 2θ = 27.4°, 54.3°, and 36.0° fit to the (110), (211), and (101) planes of the rutile phase, respectively. The average particle sizes of the TiO_2 nanoparticles in the foam were calculated using the Scherrer equation yielding approx. 17 nm for anatase and 20 nm for rutile, which is in
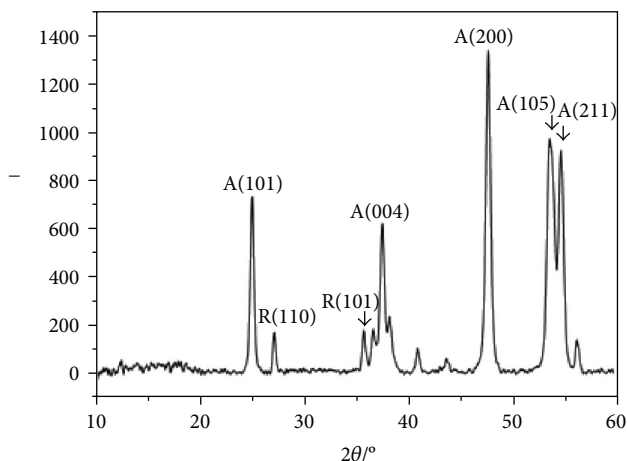
FIGURE 3: XRD pattern of the as-prepared TiO₂ foam. It is a mixture of anatase (A) and rutile (R) crystal phases.

agreement with the SEM observations. Supplementary 4 presents a comparison between the XRD pattern of TiO₂-foam-1 with original used P25 (Fig. S4) and the XRD pattern of all three samples (TiO₂-P25, TiO₂-foam-1, and TiO₂-foam-2; Fig. S5). All three samples have the same crystal structure, which is a mixture of anatase and rutile phases.

The surface composition and chemical states of the TiO₂-foam-1 and the starting TiO₂ powder (P25) were investigated by XPS. The survey spectra for both samples show exclusively the presence of C, O, and Ti (see Figure 4(a)). The Ti 2p photoelectron line (Figure 4(b)) consists of the Ti $2p_{3/2}$ and Ti $2p_{1/2}$ doublets at binding energies of 458.9 (459 eV) and 464.6 (464.7 eV), respectively. These values are closely related to the reported Ti 2p lines ranging 458.5–459.5 eV and 464.2–464.7 eV, respectively [31, 32].

The peak separation (~5.7 eV) and the strong satellite peak 14 eV above the main line indicate the Ti⁴ oxidation state. The main O 1s line (Figure 4(c)) is located at 530.1 (530.2 eV) assigned to the lattice oxygen with additional broad peak centered at 531.1 (530.9 eV) related to low coordinated surface O atoms (with low electron density than the lattice O^{2-} ions), respectively (PCCP 2000, 2, 1319–1324). The Ti : O ratios were found to be 0.48 and 0.52 for the TiO₂ foam and the P25, respectively.

3.2. Photoactivity of TiO₂ Foams.

The photoassisted degradation of NO in the gas phase was used to compare the photoactivity of the TiO₂ foams to that of the original powders (P25). The mechanism and kinetics of this reaction have been studied intensively before [9, 10]. It has been reported that using Degussa P25 as a catalyst, the determination of the reaction rate by the Langmuir–Hinshelwood model has some limitations. Wang et al. reported about the effect of variations of the inlet NO concentrations. Their observations showed that the reaction is first-order at low concentrations and zero-order at high concentrations [31, 32]. Studies conducted by Dillert et al. have shown that the NO oxidation at TiO₂ surfaces also depends on the light intensity. According to their analysis, the rates of the photocatalytic NO oxidation on UV(A)-irradiated TiO₂ samples at varying nitrogen(II)

oxide concentrations and photon fluxes and possibly at varying humidity can be predicted by a mathematical model [10].

Figure 5 shows the concentration changes of NO, NO₂, and NOₓ as a function of UV illumination time during the photoassisted oxidation of NO with employing AEROXIDE P25 and TiO₂ foam, respectively, under the same conditions. The typical experimental data for NO oxidation can be divided into four zones. Zone A is characterized by the adjustment of the NO concentration (1 ppm) before UV light illumination. Zone B is characterized by the adsorption of NO in the dark followed by the saturation of the surface of the photocatalyst sample. Once there is no further change in the NO concentration, the light source can be switched on to start the photocatalytic reaction (Zone C). After 2 h of irradiation with UV light, the light source is switched off (Zone D).

The photoassisted oxidation of NO is assumed to be a surface reaction mediated between NO and photogenerated hydroxyl radicals. And its mechanism has been already investigated. The three major steps during the photoassisted oxidation are oxidation of NO to HNO₂, oxidation of HNO₂ to NO₂ (in the transient state), and finally oxidation of NO₂ to HNO₃. If the catalyst is saturated with HNO₃, a steady state is attained and the oxidation reaction can go only as far as to NO₂ [2, 9, 10, 33, 34].

Considering the reaction dynamics during the entire photocatalytic process, the photocatalytic efficiency is determined by the number of photogenerated charge carriers which can avoid the recombination reaction. The photonic efficiency (ζ) of the NO degradation is calculated from the degradation rate of NO and the incident photon flux according to the following equation [33]:

$$\text{Photonic ef ficiency } (\zeta) = \frac{\text{degradation rate}}{\text{incident photon flux}}. \quad (1)$$

The incident photon flux (J_0) is calculated based on (2) with its value being $5 \times 10 - 8 \, \text{mol} \cdot \text{s} - 1$ (UV-A light intensity 1 mW·cm⁻², average illumination wavelength $\lambda = 350$ nm, irradiated surface area 18.49 cm², N_A Avogadro number, h Planck constant, and c light velocity).

$$J_0 = \frac{IA_r\lambda}{N_A hc}, \quad (2)$$

where I is the UV-A light intensity (1 mW·cm⁻²), A_r is the illuminated surface area (18.49 cm²), λ is the average illumination wavelength (350 nm), N_A denotes Avogadro number; h denotes Planck constant; and c denotes light velocity.

The degradation rate of NO is calculated using the following equation (where q_V is the volumetric flow rate):

$$\frac{\Delta n_{NO}}{\Delta t} = (c_{NO,in} - c_{NO,out})q_V \cdot \frac{P}{RT}. \quad (3)$$

The results are summarized and tabulated in Table 1. In this table, the results are presented as degraded concentration (C_{gas} in ppm), calculated degradation rate ($\Delta n_{NO}/\Delta t$ in mol·s⁻¹), and as photonic efficiency (ζ in %). The photonic efficiency (ζ %) for the complete degradation of the incoming
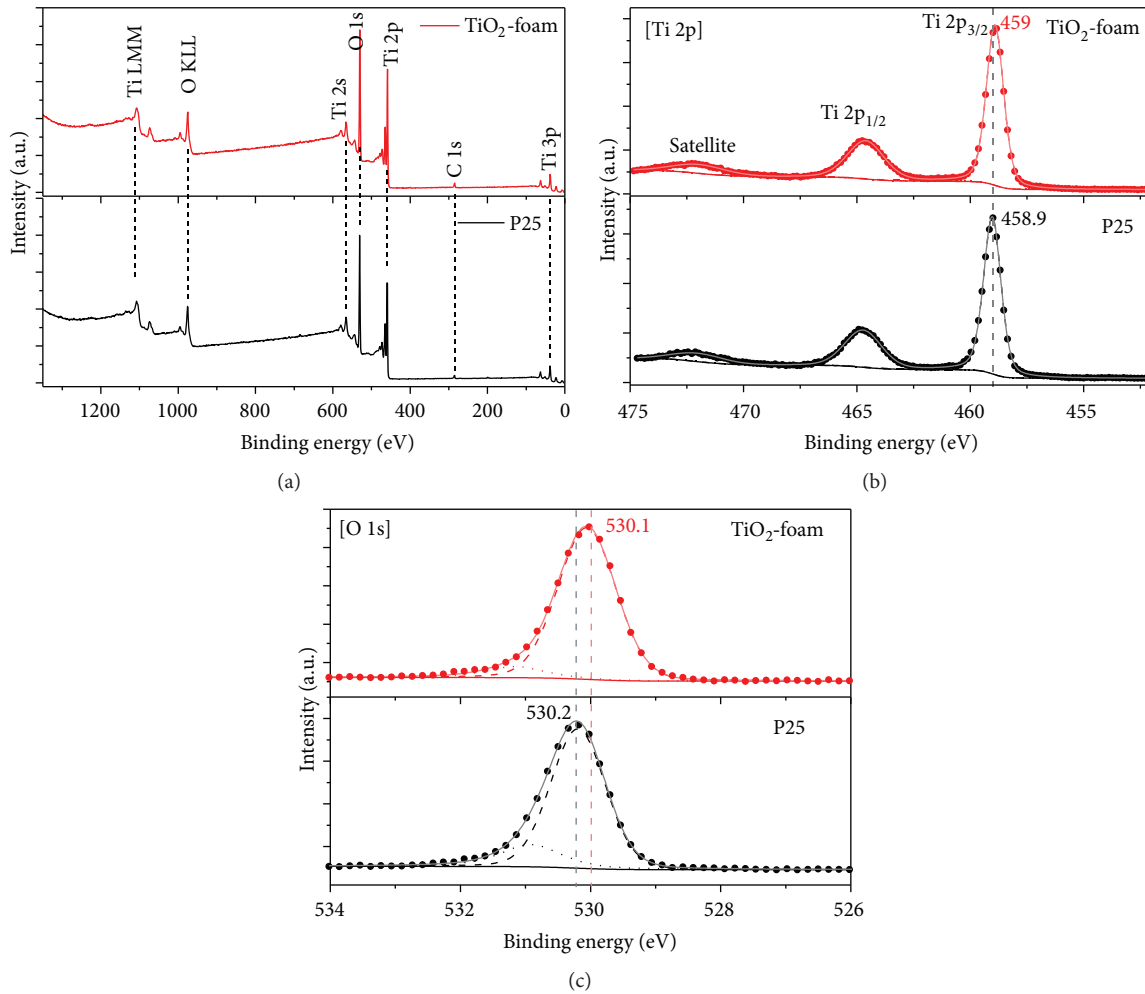
FIGURE 4: (a) XPS survey spectra of TiO_2-foam-1 and TiO_2-P25. (b) Ti 2p photoelectron line. (c) O 1s line.

NO gas under ISO 22197-1 conditions for a sample with a surface area of $18.49 \, cm^2$ is approx. 4% (for a sample with a surface area of $50 \, cm^2$, it is 1.43%).

From the results presented in Table 1, the following conclusions can be drawn: the TiO_2-foam-1 (using hexylic acid as amphiphilic molecule) adsorbs more NO than P25 powder and produces more NO_2 and NO_x (HNO_3). This could be an indication of the activity of TiO_2 foams under the UV illumination. And also it shows that the foam structures are photocatalytically more active than the original powders.

Engel et al. [30] published an experimental method for the determination of the photocatalytic deposition velocity. To gain more information about our samples and their differences, we used this method. For this investigation, we prepared two different TiO_2 foams (using different amphiphilic molecule) and change the amount of the probe gas (NO) during the photoassisted oxidation. The following equation has been used to calculate photocatalytic deposition velocity:

$$\frac{\ln c_{NO,out}/c_{NO,in}}{c_{NO,out} - c_{NO,in}} = AkiKi \cdot \frac{A_r}{q_V(c_{NO,out} - c_{NO,out})} - Ki. \quad (4)$$

This equation is a linear equation of the two variables $\ln(c_{NO,out}/c_{NO,in})/(c_{NO,out} - c_{NO,in})$ and $A_r/(q_V(c_{NO,out} - c_{NO,out}))$ having the slope $AkiKi$ and the intercept with the ordinate K_i. With the calculation of the slope, the photocatalytic deposition velocity will be determined.

Figure 6 presents the change of the NO concentration at the reactor outlet during irradiation of AEROXIDE P25, TiO_2-foam-1(with hexylic acid), and TiO_2-foam-2 (with hexylamine) with varying NO inlet concentrations. All other experimental parameters, that is, temperature, relative humidity, and UV (A) photon flux, were kept constant during these experimental runs. With the value of illumination surface area A_r ($3.96 \cdot 10^{-3} \, m^2$), the volumetric flow rate q_V ($3.0 \, L \, min^{-1}$), and the measured values of the NO inlet and outlet concentration, the values of the two variables of (4) have been calculated and plotted for each individual experimental run. These plots clearly show that the TiO_2-foam-2 (with hexylamine) has the more active surface for the NO oxidation and both foams are photocatalytically more active than the original powders.

The photoactivity depends on various factors such as the employed catalyst, the light collection efficiency, and the rate
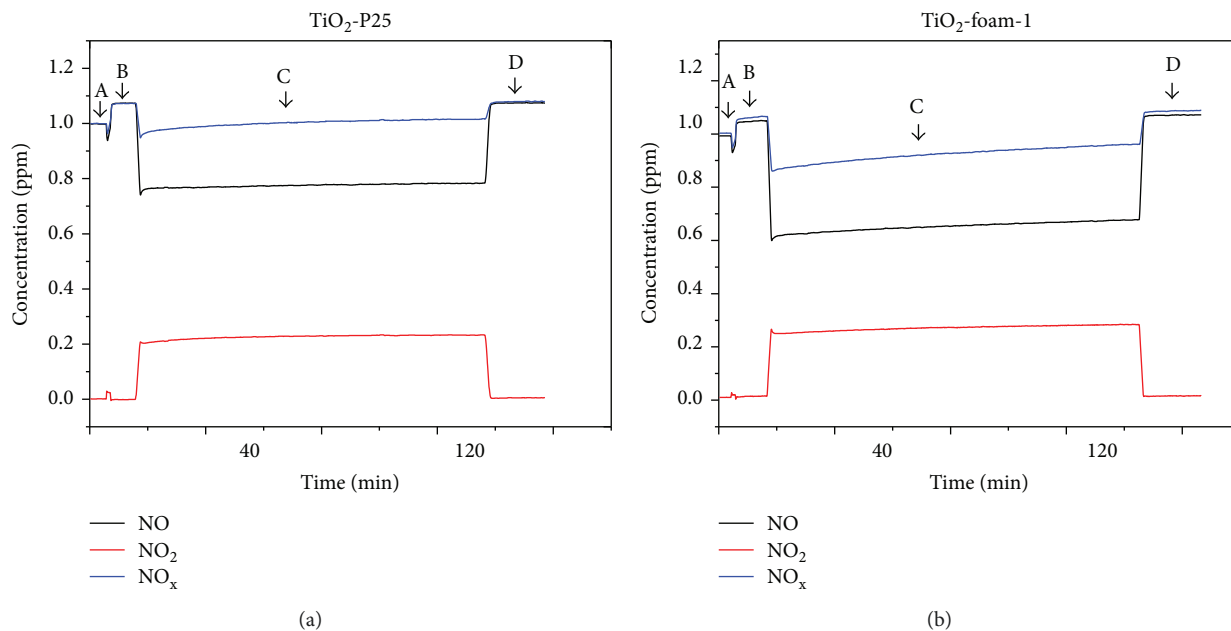
FIGURE 5: Concentration changes of NO, NO$_2$, and NO$_x$ as a function of UV illumination time in a typical experimental run for a AEROXIDE P25 (a) and TiO$_2$-foam-1 (with hexylic acid) sample (b).

TABLE 1: Concentration changes and calculated photonic efficiencies (ζ%).

Sample	ΔC_{NO} (ppm)	ΔC_{NO_x} (ppm)	ΔC_{NO2} (ppm)	$\Delta n_{NO}/\Delta t$ (10^{-10} mol·S^{-1})	ζ%
TiO$_2$ P25	0.3	0.1	0.2	6.26	1.4
TiO2-foam-1*	0.5	0.2	0.3	10.4	1.9

*Hexylic acid as amphiphilic molecule.

of molecular diffusion [7, 33, 35]. The activities of catalysts with the same chemical compositions (P25) have been compared (Table 1 and Figure 5). The light intensity for all experiments was the same although the light collection by the catalyst could be influenced by its structure. The interesting point from our results is that due to the macroporous/mesoporous structure of the foam, the photocatalyst did not own large surface area. The N$_2$ sorption results could not show big difference between the surface area of P25 and that of the foams. Although there is no big difference between the surface areas, the foam structures show more photoactivity.

TiO$_2$ foam shows high photoactivity due to the structure of macroporous/mesoporous channels that provide fast intraparticle molecular transfers, which improves the light harvesting and the adsorption of reactant molecules. This macroporous/mesoporous structure also provides proper interfaces for a facile interparticle charge transfer while the reactants can freely diffuse through the pores. At the same time, the light absorption and the energy transfer through the foam structure into the inner surface of the macroporous/mesoporous TiO$_2$ are apparently as high as expected.

It has been shown that mass transfer and surface reactions control heterogeneous catalytic reactions [10, 36]. Yang et al. [35] reported that the mass transfer coefficient is affected by the flow velocity. Beyond a certain flow velocity, the photocatalytic reaction process was founded to be independent of the mass transfer and was only controlled by the surface reactions. In this work, the value of the flow velocity is rather high and identical for all reactions. Therefore, the photocatalytic process is apparently independent of any mass transfer limitations and will only be influenced by surface properties.

The surface properties of the photocatalyst play an important role as heterogeneous photocatalytic reactions usually take place at the interface of solid/liquid or solid/gas phases. The large surface of the foam structure is apparently very effective due to the fact that the photoassisted oxidation of NO in the gas phase requires the adsorption of the reactants at the TiO$_2$ surface. The amount of adsorbed substances increases in the TiO$_2$ foam and thus enhancing the photocatalytic process.

4. Conclusions

Titanium dioxide foam was prepared by a simple mechanical stirring method. The obtained TiO$_2$ foam has been characterized using X-ray powder diffraction and SEM. The crystal structure of the TiO$_2$ foam remains unchanged as compared with the initial TiO$_2$ particles. The SEM investigations showed very rough and porous surface structures of the TiO$_2$ foam. These macroporous/mesoporous foams were used to measure the photoassisted degradation of NO according to ISO 22197-1. The photocatalytic properties of the TiO$_2$ foam, compared to those
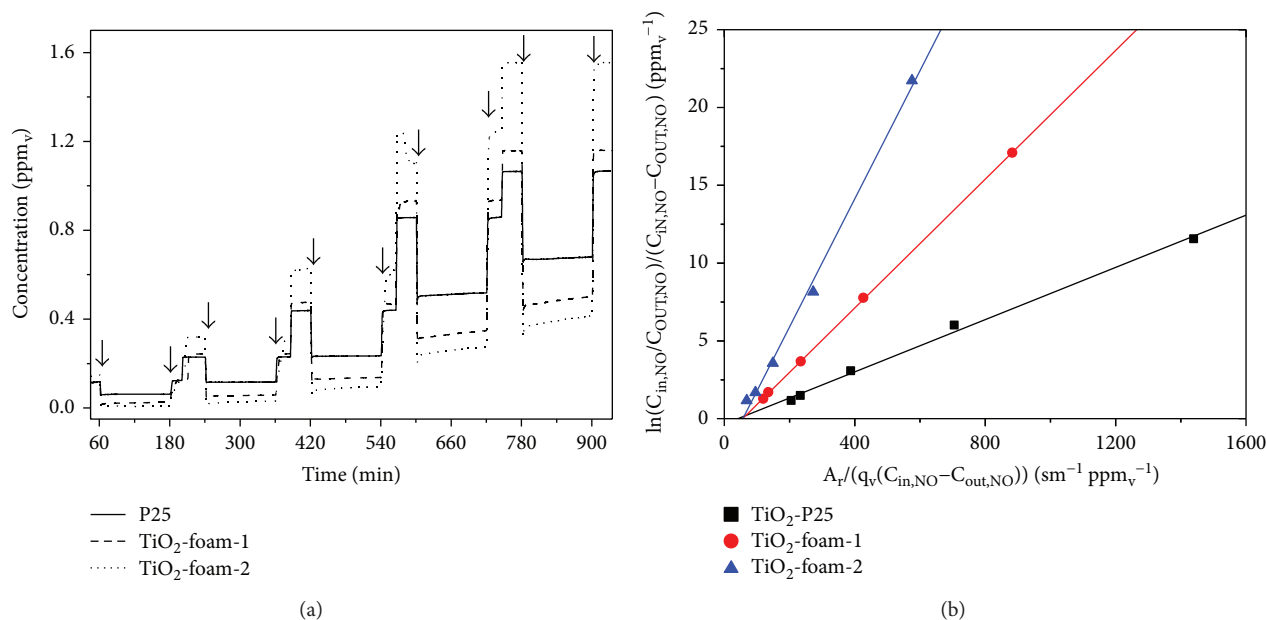
(a)

(b)

FIGURE 6: (a) Concentration changes of NO at the reactor outlet observed during three typical experimental run for a AEROXIDE P25, TiO$_2$-foam-1 (with hexylic acid), and TiO$_2$-foam-2 (with hexylamine) as a function of UV illumination. The arrows indicate switching on and off the radiation source. (b) The data analysis according to (4).

of the original photocatalyst powder, improved significantly and increased by about 135%. The photocatalytic properties of TiO$_2$ materials do not only depend on their chemical composition but also on their geometrical microstructure. The porous structure is an attractive way to achieve high photocatalytic activities.

Conflicts of Interest

The authors declare that they have no conflicts of interest.

Acknowledgments

Supplementary Materials

Supplementary 1. Fig. S1: (a) SEM photographs of TiO$_2$-P25 (Evonik AEROXIDE P25) with different magnifications. (b) SEM photographs of TiO$_2$-foam-1 (hexylic acid as amphiphilic molecule) with different magnifications. (c) SEM photographs of TiO$_2$-foam-2 (hexylamine as amphiphilic molecule) with different magnifications. Supplementary 2. Fig. S2: comparison between the diffuse reflectance spectra of TiO$_2$-P25 and prepared TiO$_2$ foam. Inset shows the modified Kubelka-Munk function versus the photon energy of these two samples. Supplementary 3. Fig. S3: left: nitrogen

adsorption-desorption isotherm of TiO$_2$-foam-1 (hexylic acid as amphiphilic molecule), TiO$_2$-foam-2 (hexylamine as amphiphilic molecule), and TiO$_2$-P25; right: the BJH graphs indicated corresponding pore size distributions of samples. Supplementary 4. Fig. S4: comparison between the XRD pattern of TiO$_2$ foam (with hexylic acid) and commercial used TiO$_2$ (Evonik AEROXIDE P25). Fig. S5: XRD patterns of TiO$_2$-P25, TiO$_2$-foam-1, and TiO$_2$-foam-2, the respective reflection peaks of anatase (A) and rutile (R) phases are labeled with their Miller indices. *(Supplementary Materials)*

References

[1] M. R. Hoffmann, S. T. Martin, W. Choi, and D. W. Bahnemann, "Environmental applications of semiconductor photocatalysis," *Chemical Reviews*, vol. 95, no. 1, pp. 69–96, 1995.

[2] X. Chen and S. S. Mao, "Titanium dioxide nanomaterials: synthesis, properties, modifications, and applications," *Chemical Reviews*, vol. 107, no. 7, pp. 2891–2959, 2007.

[3] A. O. Ibhadon, G. M. Greenway, Y. Yue, P. Falaras, and D. Tsoukleris, "The photocatalytic activity of TiO$_2$ foam and surface modified binary oxide titania nanoparticles," *Journal of Photochemistry and Photobiology A: Chemistry*, vol. 197, no. 2-3, pp. 321–328, 2008.

[4] L. Chen, C. Huang, G. Xu, S. L. Hutton, and L. Miao, "Macroporous TiO$_2$ foam with mesoporous walls," *Materials Characterization*, vol. 75, pp. 8–12, 2013.

[5] K. Skalska, J. S. Miller, and S. Ledakowicz, "Trends in NO$_x$ abatement: a review," *Science of The Total Environment*, vol. 408, no. 19, pp. 3976–3989, 2010.

[6] Z. Wu, Z. Sheng, Y. Liu, H. Wang, N. Tang, and J. Wang, "Characterization and activity of Pd-modified TiO$_2$ catalysts

for photocatalytic oxidation of NO in gas phase," *Journal of Hazardous Materials*, vol. 164, no. 2-3, pp. 542–548, 2009.

[7] Y. Ohko, Y. Nakamura, A. Fukuda, S. Matsuzawa, and K. Takeuchi, "Photocatalytic oxidation of nitrogen dioxide with TiO_2 thin films under continuous UV-light illumination," *The Journal of Physical Chemistry C*, vol. 112, no. 28, pp. 10502–10508, 2008.

[8] T. Ibusuki and K. Takeuchi, "Removal of low concentration nitrogen oxides through photoassisted heterogeneous catalysis," *Journal of Molecular Catalysis*, vol. 88, no. 1, pp. 93–102, 1994.

[9] R. Dillert, J. Stötzner, A. Engel, and D. W. Bahnemann, "Influence of inlet concentration and light intensity on the photocatalytic oxidation of nitrogen(II) oxide at the surface of Aeroxide® TiO_2 P25," *Journal of Hazardous Materials*, vol. 211-212, pp. 240–246, 2012.

[10] R. Dillert, A. Engel, J. Große, P. Lindner, and D. W. Bahnemann, "Light intensity dependence of the kinetics of the photocatalytic oxidation of nitrogen(II) oxide at the surface of TiO_2," *Physical Chemistry Chemical Physics*, vol. 15, no. 48, pp. 20876–20886, 2013.

[11] V. Kalousek, J. Tschirch, D. Bahnemann, and J. Rathouský, "Mesoporous layers of TiO_2 as highly efficient photocatalysts for the purification of air," *Superlattices and Microstructures*, vol. 44, no. 4-5, pp. 506–513, 2008.

[12] U. Diebold, "The surface science of titanium dioxide," *Surface Science Reports*, vol. 48, no. 5-8, pp. 53–229, 2003.

[13] T. A. Kandiel, R. Dillert, and D. W. Bahnemann, "Enhanced photocatalytic production of molecular hydrogen on TiO_2 modified with Pt–polypyrrole nanocomposites," *Photochemical & Photobiological Sciences*, vol. 8, no. 5, pp. 683–690, 2009.

[14] S. Sakthivel, M. C. Hidalgo, D. W. Bahnemann, S.-U. Geissen, V. Murugesan, and a. Vogelpohl, "A fine route to tune the photocatalytic activity of TiO_2," *Applied Catalysis B: Environmental*, vol. 63, no. 1-2, pp. 31–40, 2006.

[15] A. L. Linsebigler, A. L. Linsebigler, J. T. Yates Jr., G. Lu, G. Lu, and J. T. Yates, "Photocatalysis on TiO2 surfaces: principles, mechanisms, and selected results," *Chemical Reviews*, vol. 95, no. 3, pp. 735–758, 1995.

[16] Y. Wang, J. Li, P. Peng, T. Lu, and L. Wang, "Preparation of S-TiO_2 photocatalyst and photodegradation of L-acid under visible light," *Applied Surface Science*, vol. 254, no. 16, pp. 5276–5280, 2008.

[17] T. Ohno, M. Akiyoshi, T. Umebayashi, K. Asai, T. Mitsui, and M. Matsumura, "Preparation of S-doped TiO_2 photocatalysts and their photocatalytic activities under visible light," *Applied Catalysis A: General*, vol. 265, no. 1, pp. 115–121, 2004.

[18] S. U. M. Khan, M. Al-Shahry, and W. B. Ingler, "Efficient photochemical water splitting by a chemically modified n-TiO_2," *Science*, vol. 297, no. 5590, pp. 2243–2245, 2002.

[19] R. Asahi, T. Morikawa, T. Ohwaki, K. Aoki, and Y. Taga, "Visible-light photocatalysis in nitrogen-doped titanium oxides," *Science*, vol. 293, no. 5528, pp. 269–271, 2001.

[20] H. Kisch, L. Zang, C. Lange, W. F. Maier, C. Antonius, and D. Meissner, "Modified, amorphous titania—a hybrid semiconductor for detoxification and current generation by visible light," *Angewandte Chemie International Edition*, vol. 37, no. 21, pp. 3034–3036, 1998.

[21] A. A. Ismail, A. Hakki, and D. W. Bahnemann, "Mesostructure Au/TiO_2 nanocomposites for highly efficient catalytic reduction of *p*-nitrophenol," *Journal of Molecular Catalysis A: Chemical*, vol. 358, pp. 145–151, 2012.

[22] A. A. Ismail, D. W. Bahnemann, and S. A. Al-Sayari, "Synthesis and photocatalytic properties of nanocrystalline Au, Pd and Pt photodeposited onto mesoporous RuO_2-TiO_2 nanocomposites," *Applied Catalysis A: General*, vol. 431-432, pp. 62–68, 2012.

[23] J. Tschirch, D. Bahnemann, M. Wark, and J. Rathouský, "A comparative study into the photocatalytic properties of thin mesoporous layers of TiO_2 with controlled mesoporosity," *Journal of Photochemistry and Photobiology A: Chemistry*, vol. 194, no. 2-3, pp. 181–188, 2008.

[24] Y. Zhao, X. Zhang, J. Zhai et al., "Ultrastable TiO_2 foams derived macro-/meso-porous material and its photocatalytic activity," *Microporous and Mesoporous Materials*, vol. 116, no. 1-3, pp. 710–714, 2008.

[25] A. A. Ismail, D. W. Bahnemann, J. Rathousky, V. Yarovyi, and M. Wark, "Multilayered ordered mesoporous platinum/titania composite films: does the photocatalytic activity benefit from the film thickness?," *Journal of Materials Chemistry*, vol. 21, no. 21, pp. 7802–7810, 2011.

[26] T. A. Kandiel, A. A. Ismail, and D. W. Bahnemann, "Mesoporous TiO_2 nanostructures: a route to minimize Pt loading on titania photocatalysts for hydrogen production," *Physical Chemistry Chemical Physics*, vol. 13, no. 45, pp. 20155–20161, 2011.

[27] A. A. Ismail and D. W. Bahnemann, "One-step synthesis of mesoporous platinum/titania nanocomposites as photocatalyst with enhanced photocatalytic activity for methanol oxidation," *Green Chemistry*, vol. 13, no. 2, pp. 428–435, 2011.

[28] J. I. Langford and A. J. C. Wilson, "Scherrer after sixty years: a survey and some new results in the determination of crystallite size," *Journal of Applied Crystallography*, vol. 11, no. 2, pp. 102–113, 1978.

[29] ISO 22197-1, *Fine Ceramics (advanced ceramics, advanced technical ceramics) – Test Method for Air-Purification Performance of Semiconducting Photocatalytic Materials*, Part 1. Removal of Nitric Oxide, Draft International Organization for Standardization, 2007, https://www.iso.org/obp/ui/#iso:std:iso:22197:-1:ed-2:v1:en.

[30] A. Engel, A. Glyk, A. Hülsewig, J. Große, R. Dillert, and D. W. Bahnemann, "Determination of the photocatalytic deposition velocity," *Chemical Engineering Journal*, vol. 261, pp. 88–94, 2015.

[31] M. C. Biesinger, B. P. Payne, A. P. Grosvenor, L. W. M. Lau, A. R. Gerson, and R. S. C. Smart, "Resolving surface chemical states in XPS analysis of first row transition metals, oxides and hydroxides: Cr, Mn, Fe, Co and Ni," *Applied Surface Science*, vol. 257, no. 7, pp. 2717–2730, 2011.

[32] G. Ketteler, S. Yamamoto, H. Bluhm et al., "The nature of water nucleation sites on TiO_2(110) surfaces revealed by ambient pressure X-ray photoelectron spectroscopy," *The Journal of Physical Chemistry C*, vol. 111, no. 23, pp. 8278–8282, 2007.

[33] S. Devahasdin, C. Fan, K. Li, and D. H. Chen, "TiO_2 photocatalytic oxidation of nitric oxide: transient behavior and reaction kinetics," *Journal of Photochemistry and Photobiology A: Chemistry*, vol. 156, pp. 161–170, 2003.

[34] H. Wang, Z. Wu, W. Zhao, and B. Guan, "Photocatalytic oxidation of nitrogen oxides using TiO_2 loading on woven glass fabric," *Chemosphere*, vol. 66, no. 1, pp. 185–190, 2007.

[35] L. Yang, A. Cai, C. Luo, Z. Liu, W. Shangguan, and T. Xi, "Performance analysis of a novel TiO$_2$-coated foam-nickel PCO air purifier in HVAC systems," *Separation and Purification Technology*, vol. 68, no. 2, pp. 232–237, 2009.

[36] C. A. Bignozzi, "Topics in current chemistry," in *Photocatalysis*, Springer-Verlag, Berlin, Heidelberg, 2011.